Integration of speckle de-noising and image segmentation using Synthetic Aperture Radar image for flood extent extraction

J Senthilnath[1], H Vikram Shenoy[2], Ritwik Rajendra[2], S N Omkar[1,*], V Mani[1] and P G Diwakar[3]

[1]*Department of Aerospace Engineering, Indian Institute of Science, Bangalore 560 012, India.*
[2]*Department of Electronics and Communication Engineering, National Institute of Technology Karnataka, Surathkal, Mangalore 575 025, India.*
[3]*Earth Observation System, ISRO Head Quarters, Bangalore, India.*
[*]*Corresponding author. e-mail: omkar@aero.iisc.ernet.in*

Flood is one of the detrimental hydro-meteorological threats to mankind. This compels very efficient flood assessment models. In this paper, we propose remote sensing based flood assessment using Synthetic Aperture Radar (SAR) image because of its imperviousness to unfavourable weather conditions. However, they suffer from the speckle noise. Hence, the processing of SAR image is applied in two stages: speckle removal filters and image segmentation methods for flood mapping. The speckle noise has been reduced with the help of Lee, Frost and Gamma MAP filters. A performance comparison of these speckle removal filters is presented. From the results obtained, we deduce that the Gamma MAP is reliable. The selected Gamma MAP filtered image is segmented using Gray Level Co-occurrence Matrix (GLCM) and Mean Shift Segmentation (MSS). The GLCM is a texture analysis method that separates the image pixels into water and non-water groups based on their spectral feature whereas MSS is a gradient ascent method, here segmentation is carried out using spectral and spatial information. As test case, Kosi river flood is considered in our study. From the segmentation result of both these methods are comprehensively analysed and concluded that the MSS is efficient for flood mapping.

1. Introduction

With the onset of drastic climate conditions, floods being one of the most devastating natural hazards are of paramount concern these days. So we need an effective flood assessment model which should be able to extract the maximum information during the flood peak. Present methods employ satellite images to extract flood inundation extent. Optical images obtained from the satellites are often prone to bad climatic conditions and hence there is a possibility of misinterpretation of land cover map under the cloudy weather conditions. However, Synthetic Aperture Radar (SAR) is an active microwave instrument, producing imagery of the Earth's surface at any time instant (day or night)

Keywords. Synthetic Aperture Radar; flood assessment; speckle filters; gray level co-occurrence matrix; mean shift segmentation.

J. Earth Syst. Sci. **122**, No. 3, June 2013, pp. 559–572

and in all weather conditions; hence it is often used for monitoring the flood event (Chunming *et al.* 2005).

The major challenge associated with the SAR image processing is the presence of speckles (Lee 1981). This affect spectral characteristic which is due to coherent interference of waves scattered from terrain elements. Thus make texture analysis of such images difficult. It also affects the spatial characteristics of the backscatter in underlying scene. Consequently, it reduces the efficiency of image classification (Durand *et al.* 1987). The SAR backscattering coefficient is affected by several parameters like incidence angle, polarization, surface roughness and dielectric constant. The uneven roughness during flood because of high winds and submerged vegetation causes hurdle in SAR image processing (Huang 2008). The dielectric constant of materials is analogous to its reflectance, and hence influences its appearance in a SAR image (Freeman and Durden 1998). As dielectric constant represents the amount of absorption, materials with higher dielectric constants appear dark in radar images. The water has very high dielectric constant and thus it appears dark.

In order to effectively analyse the image, we need to reduce speckle noise to a great extent possible, which is achieved through filtering. But filtering not only reduces the speckle noise, but also leads to degradation of the image depending on the extent of smoothing done by the filter (Sheng and Xia 1996). In addition to speckle suppression, an ideal filter must preserve edges and texture information. In the literature, adaptive filters for speckle removal are preferred for this purpose, since most of the well-known speckle removal filters perform the calculation of the local observed mean along with normalized standard deviation. This effectively suppresses noise thus preserving edges and textures. Different methods have been developed for filtering SAR image namely Lee filter (Lee 1981), Frost filter (Frost *et al.* 1982) and Gamma MAP filter (Lopes *et al.* 1990).

In past decades, researchers have used SAR images for monitoring the flood. Chenghu *et al.* (2000) presented RBF neural network method integrated with a spectral-vector model for automatic extraction of flooded areas. Kussul *et al.* (2008) used self-organizing Kohonen maps to monitor flood conditions along with ortho-rectification using DEM. Also, some of the researchers have considered both SAR (during flood) and optical images (before flood) for flood assessment. An analysis of flood inundation risks in terms of land use has been done (Duc 2006). In their study, Gray Level Co-occurrence Matrix (GLCM) was used for texture analysis and then supervised method namely maximum likelihood classifier was used for flooded area segmentation. A hybrid methodology for flood assessment is proposed by Matgen *et al.* (2011). They incorporated radiometric thresholding and region growing method to analyse the flood extent. Patel *et al.* (2009) presented GLCM based texture analysis for single look high resolution SAR data.

There have been several models and classification methods proposed for the flood assessment (Kussul *et al.* 2008; Matgen *et al.* 2011). Texture analysis is one such method, which uses GLCM to provide a measure of variation of intensity levels (Shamaomaa *et al.* 2006). Flood boundary detection of SAR images using GLCM parameters like entropy and angular moment was presented (Chunming *et al.* 2005). Sharp variations between the texture of water bodies and non-water bodies are considered in their analysis. Also, GLCM and Holder exponent is used by Chakraborty *et al.* (2009) for satellite image segmentation.

Mean shift segmentation (MSS) is a non-parametric technique which is often used in the field of pattern recognition. The main advantage of MSS is that it doesn't need prior knowledge of number of clusters unlike K-means. Jarabo *et al.* (2011) presented mean shift segmentation for processing SAR images by considering both spatial and range distribution. Also for multi-modal feature space analysis of images, robust mean shift procedure has been employed (Comaniciu and Meer 2002).Though mean shift clustering is a trivial image segmentation technique, it fails in its robustness because of the presence of speckle noise in SAR images (Jarabo *et al.* 2011).

In this paper, we propose a two-stage method of flood inundation extraction using SAR image because of its aforementioned improvements over the optical image. At first stage, pre-processing of input image is done to filter the speckle noise. For this purpose, performance comparison of different speckle removal filters is done. At second stage, as a part of image segmentation, GLCM and mean shift segmentation are applied on filtered image for flood mapping. Comparative study of both the image segmentation methods has been done to analyse flood extent with reference to ground truth in terms of discharge and accuracy. Also, analysis of land cover regions affected by flood is depicted using Linear Imaging Self Scanning sensor (LISS-III) image.

The remainder of this paper is organized as follows: Section 2 describes the speckle de-noising and segmentation approach, section 3 discusses performance evaluation, section 4 provides an overview of the study area and results. Conclusions and discussions are presented in section 5.

2. Methodology

Different methods of speckle removal filters and image segmentation methods for flood mapping are described in this section. The flow chart of the proposed method is shown in figure 1.

2.1 *Image pre-processing*

In this subsection, we explicate about how each speckle removal filter works. As SAR image processing is quite difficult because of the presence of speckles, there is a need for filtering as a pre-processing step. These filters employ kernel window of size $X * Y$ that move over each pixel in the image by applying a mathematical calculation using the pixel values under the kernel. The value of reference pixel is replaced by the calculated value. Degree of smoothing is a function of kernel window size. As filter kernel size increases, smoothing increases. For speckle removal, most widely used filters are Lee filter, Frost filter and Gamma MAP filter.

- *Lee Filter:* Speckle noise is generally assumed to be a multiplicative model, but in this filter it is approximated to an additive model to simplify calculations. Here, the filtered or output pixel value is a weighted sum of the reference pixel value and the mean of the values within the kernel (Lee 1981).
- *Frost filter:* The unspeckled pixel value is estimated using a sub-window of the processing window. The size of the sub-window varies as a function of target local heterogeneity measured with coefficient of variation; the larger the coefficient of variation, the narrower the processing sub-window.
- *Gamma MAP filter:* This filter is based on the Bayesian analysis of image statistics. It uses the Maximum A-Posteriori (MAP) estimation method. While using this filter, Gamma distribution is assumed for the underlying image and the speckle noise in it. Thus this filter works best for geo-spatial images containing homogenous areas such as oceans, forests, fields, etc. (Lopes *et al.* 1990).

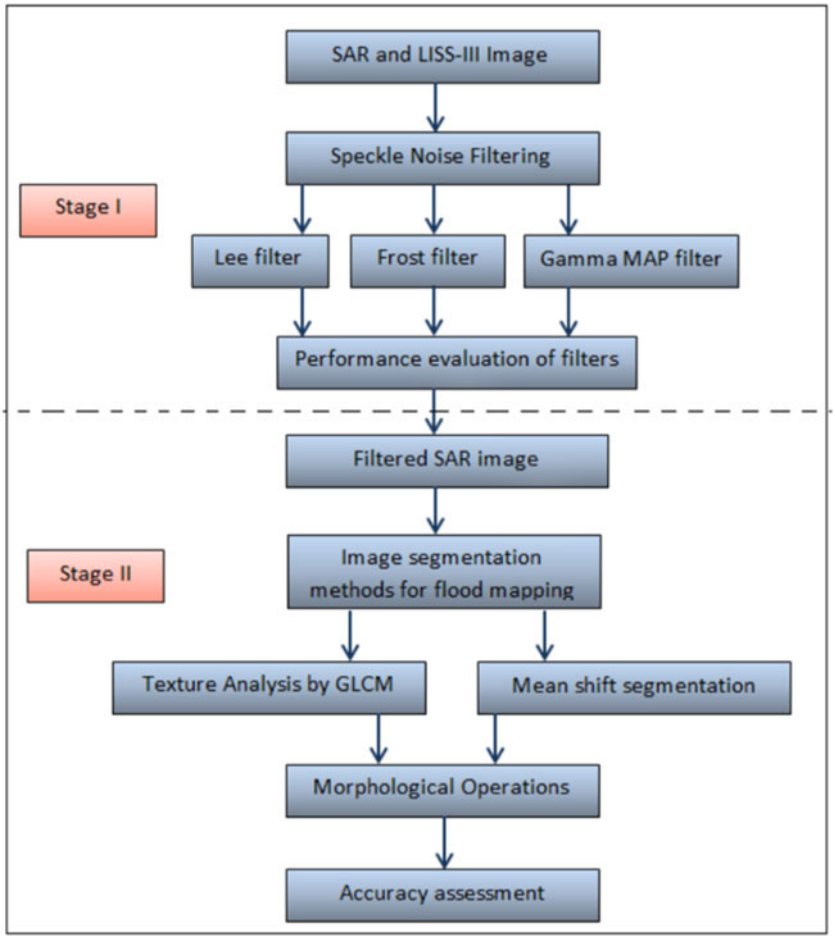

Figure 1. Flow chart of proposed methodology.

2.2 *Image segmentation methods for flood area mapping*

In this subsection, we elucidate the methods of image segmentation to derive flood extent information. GLCM as a texture analysis method and mean shift segmentation as gradient ascent method are used to serve the purpose of flood mapping.

2.2.1 *GLCM procedure for flood assessment*

In texture analysis, GLCM is an important tool for the measurement of variation in intensity levels at the pixel of interest with certain spatial relationship with the neighbouring pixels. There are several GLCM parameters like contrast, dissimilarity, mean, standard deviation, entropy and angular moment. In the literature, several GLCM texture measure parameters are exploited for single look high resolution SAR data (Srivastava *et al.* 2009). We have used entropy and angular moment for the flood extent extraction because of their opposite characteristics (Chunming *et al.* 2005). Entropy gives a measure of randomness of grey levels in an image. Entropy is low for uniform data in a given window and hence indicated by darker region and angular second moment is high for entries with almost nearby values and image is brighter in the portion of uniform entries. Hence, the texture of an image can be characterized by this contrasting feature of entropy and angular second moment. Mathematically, entropy and angular moment are calculated as:

$$\text{Entropy} = \sum_{i,j=1}^{N} -P_{i,j} \cdot \log_2(P_{i,j}) \tag{1}$$

$$\text{Angular moment} = \sum_{i,j=1}^{N} (P_{i,j})^2 \tag{2}$$

where $P_{i,j}$ is an element of normalized symmetrical GLCM and N is the number of grey levels in an image.

Better accuracy and the effect of averaging of texture properties need to be considered for choosing optimal window size. Once the entropy and angular moment are calculated, output image pixel is replaced by the entropy and angular moment of $M * M$ neighbourhood of corresponding input image pixel to get entropy-filtered and energy-filtered image. Pixel value of energy-filtered image over that of entropy-filtered image gives us the ratio image. The ratio image is further processed using morphological operation to extract flood prone region.

2.2.2 *Mean shift segmentation for flood assessment*

Mean shift algorithm is a non-parametric segmentation technique. It does not need any prior information on the number of clusters or shape of the clusters to be formed (Konstantinos 2005). The basic concept of mean shift segmentation algorithm is to treat the data points in d-dimensional feature space as an empirical probability density function. Dense regions correspond to local maxima (modes) of a distribution function. In our study, we have used Gaussian kernel function which is defined by

$$K(x) = C_k * \exp\left(-x^2\right) \tag{3}$$

where x is a vector of data points and C_k is the normalization constant which makes the integral of the kernel function as 1.

Since we are implementing the mean shift algorithm on image dataset, each sample is described by its spatial domain (position in the image) and the range domain (grey level intensities). Thus, two kernel functions are used for image segmentation, where h_r and h_s are the bandwidth in range and spatial domain respectively.

For the samples x_1, x_2, $x_3, \ldots, x_n$, the density estimation function is given by (Jarabo *et al.* 2011)

$$f(x) = \frac{\sum_{i=1}^{N} x_i k\left(\frac{x-x_i}{h_r}\right) * k\left(\frac{x-x_i}{h_s}\right)}{n * h_r * h_s}. \tag{4}$$

Then, convergence is verified by obtaining the density gradient ascent estimated to be zero.

Only the points which lie inside the kernel defined by h_s and h_r contribute to the density estimation function. To analyse the feature space, we have to locate the zeros of density gradient estimation. Also, we define a function $g(x) = -k'(x)$, and $G(x) = C_k g(|x|^2)$, $K(x)$ being shadow function of $G(x)$. Advantage of mean shift procedure is that it allows us to find the zeros of the density gradient without estimating the probability density function. Mean shift vector $m(x)$ is calculated using (Jarabo *et al.* 2011)

$$m(x) = \frac{\sum_{i=1}^{i=N} x_i \cdot g\left(\left\|\frac{x-x_i}{h}\right\|^2\right)}{\sum_{i=1}^{i=N} g\left(\left\|\frac{x-x_i}{h}\right\|^2\right)} - x. \tag{5}$$

Mean shift is calculated until the convergence. The condition of convergence that we have used is maximum number of iterations.

Mean shift procedure for flood assessment is as follows:

- The input SAR image is mapped into feature space. Here it is one-dimensional, since we are dealing with grey scale image.

- Adequate number of kernel windows are defined at random locations in feature space. Kernel function is expressed in equation (3). It is assigned with spatial and range bandwidths. Here, spatial refers to the position of the image pixels and range domain refers to the grey scale intensity levels.
- For each kernel window, the modes or centres of high density regions are calculated using equation (5).
- Each intensity level is shifted towards the mode until convergence. Maximum number of iterations is used as a criterion for convergence.
- High density regions in the feature space are mapped into corresponding regions in the image domain.
- Morphological operations are done on the segmented image as a part of post processing.

The performance of filters and image segmentation methods are evaluated based on certain parameters which are explained in the following section.

3. Performance evaluation

A speckle suppression filter is expected to filter the homogeneous areas with reasonable speckle reduction capability, retain edges and preserve features. For the purpose of evaluating the performance of the filters in de-speckling the SAR image, we use the following criteria: mean square error, signal-to-noise ratio (Mansourpour *et al.* 2006) and speckle suppression index (Sheng and Xia 1996).

3.1 *Performance evaluation of speckle removal filters*

3.1.1 *Mean square error (MSE)*

MSE is the measure of the extent to which the output image differs from the input image. This helps indirectly to assess the feature preservation.

$$\mathrm{MSE} = \frac{1}{K} \times \left(\sum S_i(n) - S_o(n) \right) \tag{6}$$

where S_i is the noisy input image, S_o is the filtered output image and K is the size of the image. Accurate filtering of images with high noise content could also lead to large values of MSE.

3.1.2 *Signal-to-noise ratio (SNR)*

SNR gives the strength of the pure signal or image, as compared to the noise present which is removed by the filter.

$$\mathrm{SNR} = 10 \log_{10} \left(\sum \frac{S_o(n)}{(S_i(n) - S_o(n))^2} \right) \tag{7}$$

Higher SNR emulates better performance.

3.1.3 *Speckle suppression index (SSI)*

The ability of the filter to suppress the speckle is measured in terms of standard deviation of the image to its mean intensity.

$$\mathrm{SSI} = \frac{\left(\frac{\mathrm{std}(S_o)}{\mathrm{mean}(S_o)} \right)}{\left(\frac{\mathrm{std}(S_i)}{\mathrm{mean}(S_i)} \right)} \tag{8}$$

where std( ) refers to the standard deviation. SSI is inversely proportional to the suppression ability of the filter.

3.2 *Performance evaluation of image segmentation techniques*

After the speckle noise suppression evaluation, the images resulting from classification methods are appraised with suitable parameters for accuracy assessment. GLCM parameters are examined for different window sizes and mean shift segmentation performance analysis is done for different bandwidths in range and spatial domain. Error matrix is tabulated in order to do the performance analysis. Accuracy assessment of these image segmentation techniques is done using user's accuracy, producer's accuracy (Gamba and Aldrighi 2012) and kappa coefficient (Stehman 1995), which are estimated from the error matrix as follows:

$$\text{User's accuracy} = \frac{\text{Flooded area properly identified in a classification method}}{\text{Total flooded area calculated from the method}} \tag{9}$$

$$\text{Producer's accuracy} = \frac{\text{Flooded area properly identified in a classification method}}{\text{Flooded area in the reference ground truth}} \tag{10}$$

$$\text{Kappa coefficient} = \frac{\text{Observed accuracy} - \text{Expected agreement}}{1 - \text{Expected agreement}} \tag{11}$$

where

$$\text{Expected agreement} = \frac{c_t * f_t + nc_t * nf_t}{(A)^2}$$

Here, c_t is the total flooded area from a classified method, f_t is actual total flooded area, nc_t is total non-flooded area from a classified method, nf_t is the actual non-flooded total area and A is the total area under study.

4. Results and discussion

In this section, we present the results obtained by classification of LISS-III image (before flood) and SAR image (during flood). Here, LISS-III image is used to analyse land cover regions and SAR image is used to extract flood prone regions.

4.1 *Study area and data description*

Our study area includes the regions affected by the Kosi river flood in Bihar in 2008. We focus mainly on the Bhagalpur district, where the Kosi tributary merges with Ganges, and assess the extent of damage caused. The region is contained within the co-ordinates: 25°39′30.76″N–86°25′54.24″E and 25°12′34.42″N–87°17′21.70″E. The districts covered include Bhagalpur, Khagaria, Katihar, Madhepur and Purnia.

We use LISS-III image to assess the land cover prior to the flood. It was collected on April 11, 2008 from RESOURCESAT-2. For flood delineation, we use SAR image C-band dataset obtained from RADARSAT-2 on August 27, 2008 during the flood. The image is of size 1614×3645 pixels. The spatial resolution of the LISS-III image used is 23.5 metres. SAR image dataset has azimuth and range pixel spacing of 25 metres each. The beam mode is ScanSAR narrow with incidence angle range of 20°–46° and polarization is of HH type. This HH polarized backscatter coefficient gives more contrast between land and water surfaces compared to VV polarization (Herrera-Cruz and Koudogbo 2009). Total area under study is 3248.9 km^2 where discharge is 1596.6 km^2 and flooded area is 1911.2 km^2. The map of the region under study is illustrated in figure 2.

4.2 *LISS-III image classification*

Classification of before flood land cover types from LISS-III image has been done using ERDAS 9.2®. Firstly, we carried out level 1 classification by generating signature file to classify the satellite image using maximum likelihood classifier. Using this supervised classification, the image is classified into four classes namely, urban land, fallow land, vegetation and water bodies. Multiple sources used

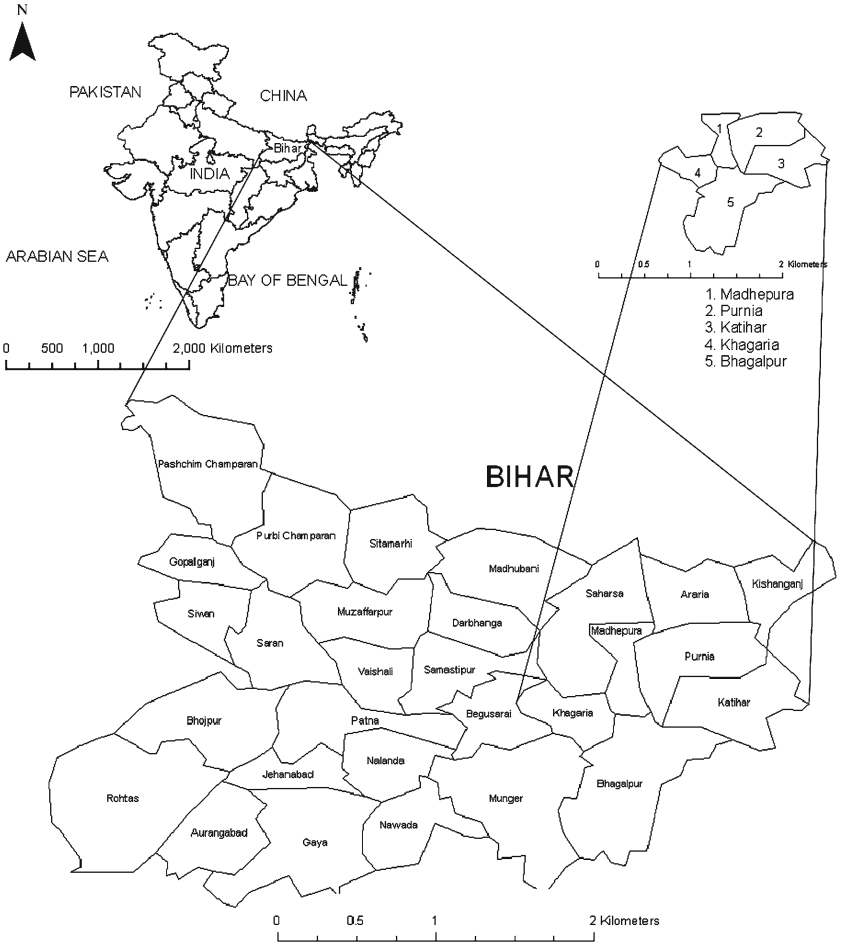

Figure 2. Study area – 5 districts, Bihar, INDIA.

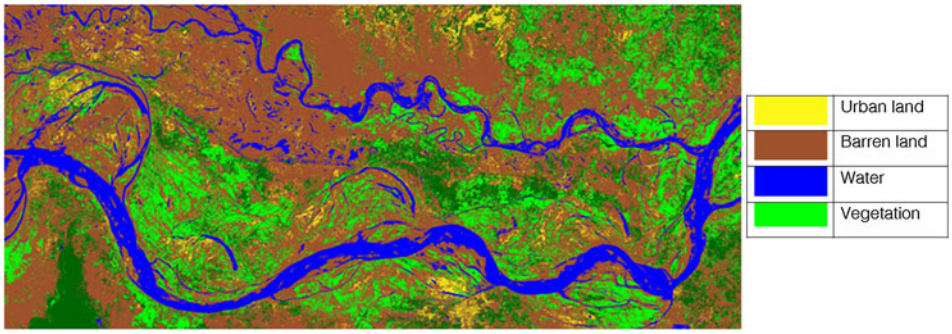

Figure 3. Land cover types classified using ERDAS 9.2.

Table 1. *Analyses of pre-flood and post-flood area of land cover types.*

Class	Before flood (km^2)	During flood (km^2)		Percentage of area flooded
		Flooded	Unflooded	
Urban land	100.7	60.0	40.7	59.59%
Barren land	2068.7	1186.4	882.3	57.35%
Vegetation	801.9	350.6	451.3	43.72%

as reference includes topographical maps, manual analysis and ground verification. Figure 3 shows the classified land cover types. From table 1, we can observe that before flood and during flood analysis of land cover regions in terms of area.

4.3 *SAR image processing*

In the first stage, speckle noise is removed and in the second stage image segmentation results are analysed for during flood image (SAR). SAR image is based on backscatter coefficient which is a function of various parameters. Radar system parameters and ground surface parameters decide the backscatter intensity. The expression for backscatter echo intensity (Huang 2008) is given in equation (12).

$$\sigma = f(\lambda, \theta, P, \varepsilon, \varphi, \Gamma_1, \Gamma_2, V) \tag{12}$$

where λ is wavelength, θ is incident angle, P polarization mode, φ is azimuth angle, ε is complex

Figure 4. Original SAR image.

dielectric constant, Γ_1 is surface roughness, Γ_2 is subsurface roughness and V is bulk scattering coefficient of inhomogeneous medium.

SAR backscatter coefficient is affected by wind induced surface roughness (Srivastava *et al.* 2006). However HH polarization is less sensitive to surface roughness caused due to strong winds (CCRS 2011), hence we could present better contrast between land and water.

4.3.1 *Speckle removal filtering*

This study aims at statistical approach of flood assessment in terms of discharge and accuracy.

Table 2. *Analysis of various speckle removal filters.*

	MSE	SNR	SSI
Gamma-MAP (3×3)	1.5943	20.6701	0.9640
Lee (3×3)	6.4820	17.9444	0.9613
Lee (5×5)	14.4388	12.0489	0.9288
Frost (3×3)	5.4510	17.8908	0.9703

Here we consider a SAR image which is shown in figure 4. Various speckle removal filters, namely Lee filters of window sizes 3×3 and 5×5, Frost filter of window size 3×3 and Gamma-MAP filter of window size 3×3 are applied on the original SAR. Thereafter histogram equalisation is performed on the filter outputs.

Performance of above-mentioned speckle removal filters have been evaluated as described in the previous section to find out the most suitable one. The results are tabulated as shown in table 2.

From table 2, we observe that although the Lee filters have better SSI, Gamma-MAP shows better performance in terms of MSE and SNR thereby indicating its superiority in terms of edge and feature preservation. For further stage, we chose Gamma MAP filter for speckle removal whose result image is shown in figure 5.

After the filtering process, segmentation based on GLCM based texture analysis and mean shift procedure are performed. Accuracy assessment of these methods is done with respect to the ground truth.

Figure 5. Gamma MAP filtered image.

Table 3. *Error matrix for the accuracy assessment.*

		Reference ground truth image (GT)		
		Flooded area (km^2)	Non-flooded area (km^2)	Total area (km^2)
Classified Map (GLCM texture based)	Flooded (GLCM)	1118.6	27.6	1146.2
	Non-flooded (GLCM)	797.6	1305.1	2102.7
	Total (GLCM)	1916.2	1332.7	3248.9

Note: Diagonal elements are properly classified elements, non-diagonal elements are misinterpreted ones.

4.3.2 *Grey level co-occurrence matrix (GLCM)*

In texture analysis, entropy is low and angular moment is high for water regions, hence these contrasting features were employed in our study. For texture analysis, different segmentation windows of 5×5, 7×7, 9×9 and 11×11 neighbourhood were tested to find out the most accurate one. For this analysis, we used the error matrix shown in table 3 to estimate the user's accuracy, producer's accuracy and kappa coefficient. We observed that 7×7 window is more appropriate for our analysis as per the results shown in table 4. These performance evaluating parameters are calculated as explained in the equations (9–11).

Figure 6 shows the result of GLCM based flood mapping. The result image is actually the ratio of pixel intensities of angular moment filtered image to that of entropy filtered one. The discharge area with different GLCM window sizes is depicted in figure 7.

From figure 6, we note that GLCM has not been successful in picking some of the flooded regions because of the similarities in texture properties of land region surrounded by the water and the flooded region. Since grey scale intensity levels are influenced by factors like surface roughness, corner reflection effect and dielectric constant, texture analysis (GLCM) still results in relatively small false change (Huang 2008).

Table 4. *Accuracy assessment of GLCM based flood mapping.*

	Segmentation window size in GLCM			
	5×5	7×7	9×9	11×11
User's accuracy	98.9498%	97.5953%	98.9612%	99.3621%
Producer's accuracy	53.2893%	58.3759%	53.7829%	50.3470%
Kappa coefficient	0.4766	0.5175	0.4816	0.4572

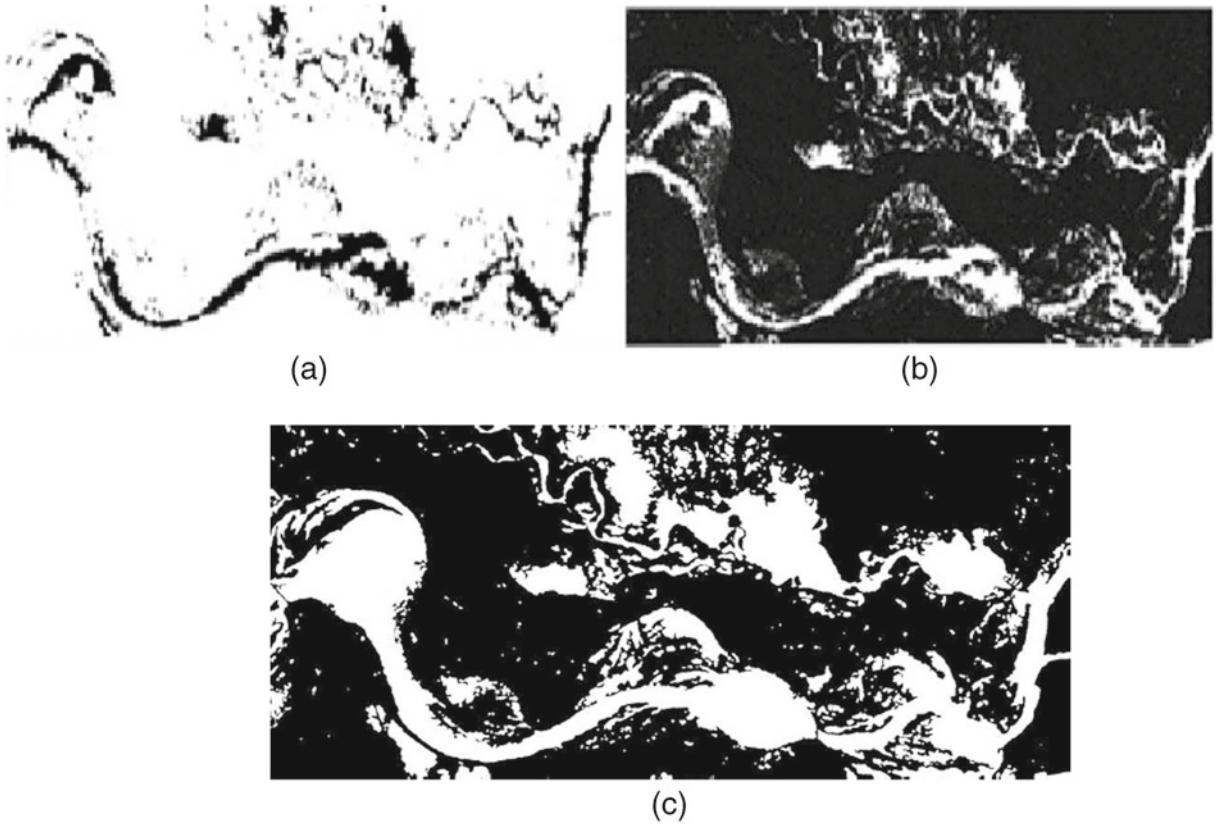

Figure 6. GLCM results. (**a**) Entropy filtered image, (**b**) energy filtered image and (**c**) ratio result image.

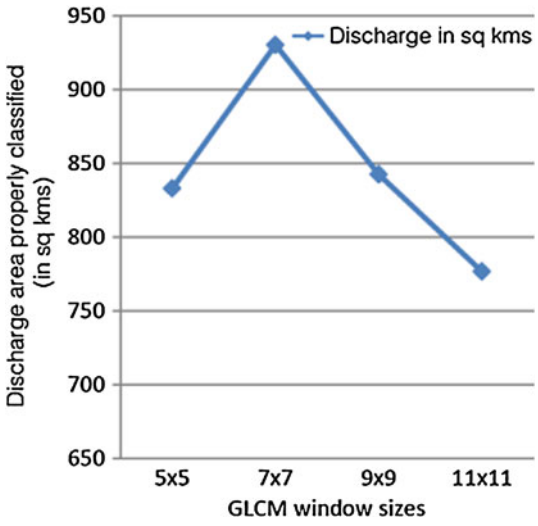

Figure 7. Discharge (in km^2) *vs.* GLCM window sizes.

4.3.3 *Mean shift segmentation for flood mapping*

Mean shift procedure is applied on the input SAR image as described in the algorithm. It is examined for different combinations of spatial and range bandwidths. The result image is shown in figure 8. Mean shift segmentation is evaluated using the error matrix shown in table 5 to calculate its user's accuracy, producer's accuracy and kappa coefficient. Table 6 shows the result interpretation of MSS for different combinations of range and spatial bandwidths. Range (h_r) and spatial (h_s) bandwidths with value as (5, 5) is observed to be relatively better compared to other bandwidth combinations. Combinations with (h_r, h_s) less than (5, 5) shows consistent results. The discharge area *vs.* bandwidth combinations is presented in figure 9.

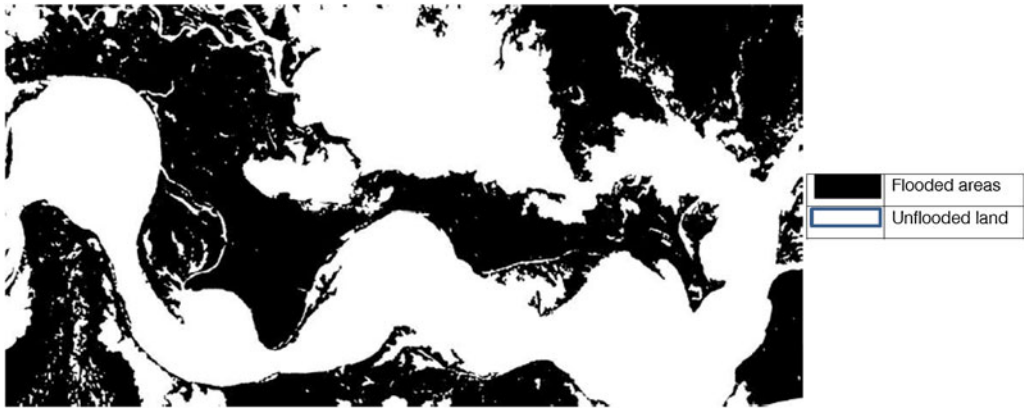

Figure 8. Mean shift segmentation based flood mapping.

Table 5. *Error matrix for MSS accuracy assessment.*

		Reference ground truth image (GT)		
Bandwidths $h_r = 5$, $h_s = 5$		Flooded area (km^2)	Non-flooded area (km^2)	Total area (km^2)
Classified Map (Mean shift segmentation based)	Flooded (MSS)	1723.1	42.2	1765.3
	Non-flooded (MSS)	193.1	1290.5	1483.6
	Total (MSS)	1916.2	1332.7	3248.9

Table 6. *Accuracy assessment of MSS for different bandwidth combinations.*

	Range and spatial bandwidth in MSS (h_r, h_s)			
	(2, 2)	(5, 5)	(10, 10)	(15, 15)
User's accuracy	97.6198%	97.6089%	97.6276%	97.6937%
Producer's accuracy	89.9144%	89.9245%	89.8762%	89.8293%
Kappa coefficient	0.8530	0.8529	0.8525	0.8528

Once the flood extent mapping is done by the image segmentation methods, the result images are overlaid on the LISS-III classified image for the analysis of flood prone land cover types. The result images are shown in figure 10.

From figure 10(a) we observe that GLCM has failed to pick the flooded regions effectively and a significant portion of flooded land has been wrongly picked as unflooded. Also, we can notice from figure 10(b) that the mean shift algorithm has picked the flooded land cover types quite effectively.

The performance of the two methods with respect to picking the flooded regions is compared with that of the ground truth. The result obtained is compared with one another, through the bar graph shown in figure 11.

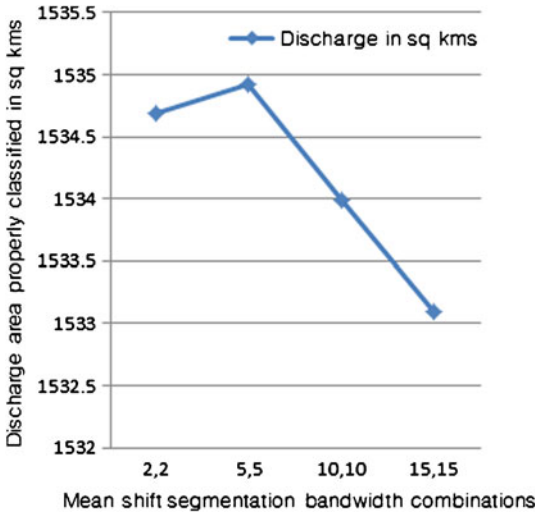

Figure 9. Discharge area *vs.* MSS bandwidth combinations.

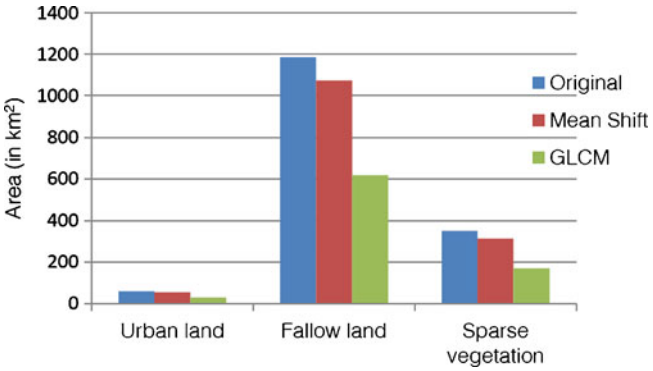

Figure 11. Comparisons of areas of land cover types.

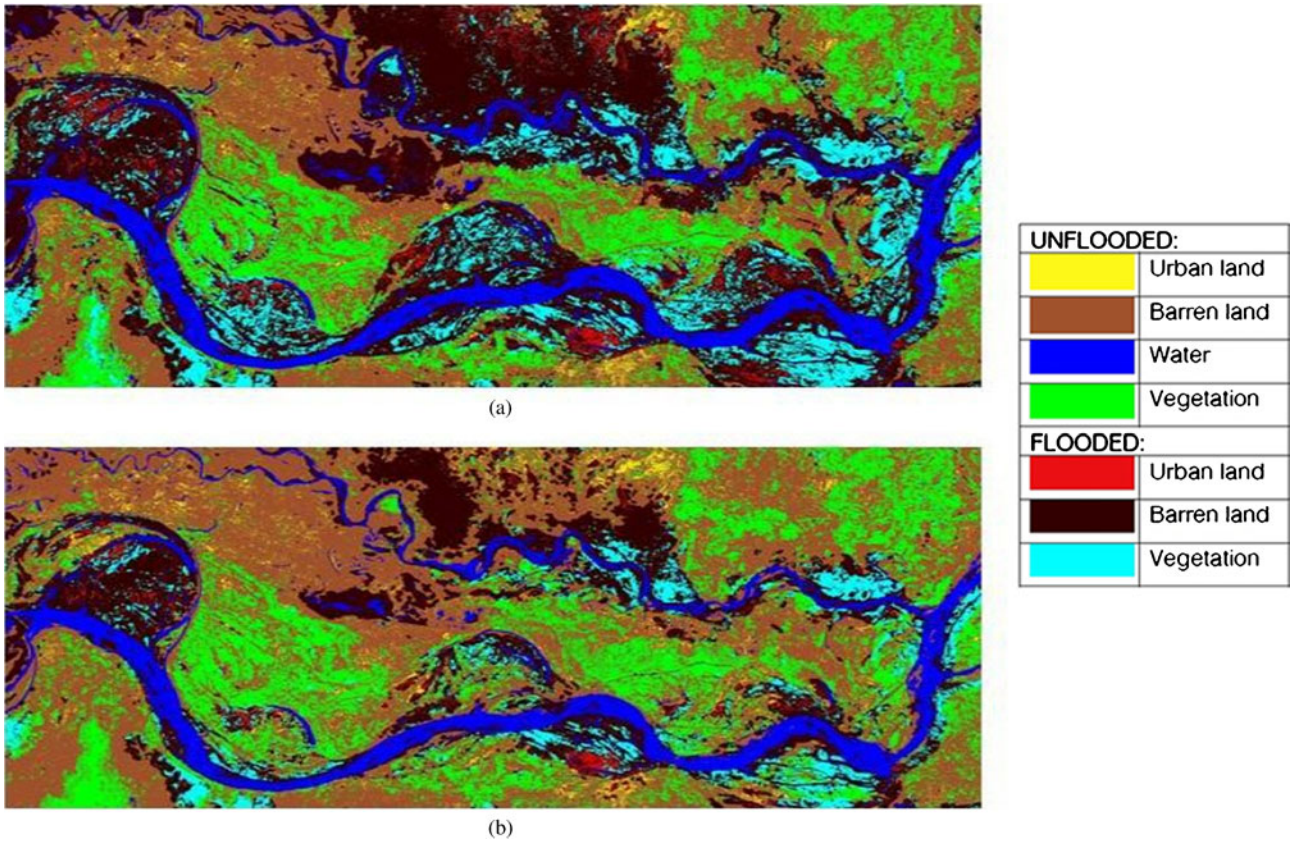

Figure 10. Land cover mapping by (**a**) GLCM and (**b**) MSS.

We have also compared the accuracy of the two methods by calculating the percentage of land cover types correctly picked by them, with respect to the ground truth. This result is shown in table 7.

Table 7. *Accuracy assessment of flooded land cover types derived from two classification methods.*

	Accuracy	
Class	MSS	GLCM
Urban land	91.06%	49.38%
Fallow land	90.48%	48.04%
Vegetation	89.43%	48.35%

From table 2, we observe that Gamma MAP filter is better than Lee and Frost filters. Further, the reason for selecting Gamma MAP filtered image for classification has been analyzed. All three filters were tested for mean shift segmentation of the SAR image for flood extent extraction, as shown in figure 12.

From table 8, we can observe the performance of various speckle removal filters in classifying the image into flooded and non-flooded regions is measured in terms of user's accuracy, producer's accuracy and kappa coefficient. The Gamma MAP filter is found to be most suitable speckle de-noising

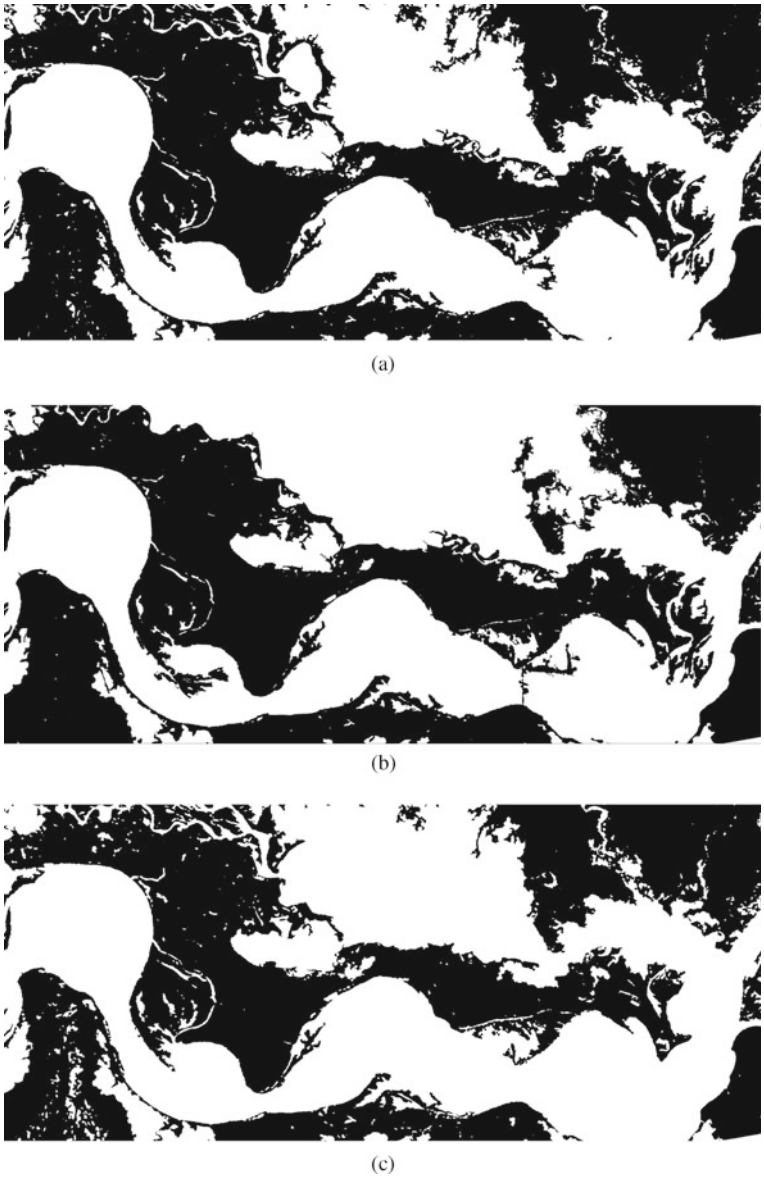

Figure 12. Mean shift segmentation results of SAR image after (**a**) Frost filtering (**b**) Lee (5×5) filtering and (**c**) Gamma MAP filtering.

Table 8. *Performance comparison of speckle de-noising filters.*

	User's accuracy	Producer's accuracy	Kappa coefficient
Lee (5×5)	92.2741	82.0809	0.7049
Frost	99.2612	82.8963	0.7915
Gamma MAP	97.6937	89.8293	0.8528

filter in terms of user's accuracy, producer's accuracy and kappa coefficient. Hence, in this study Gamma MAP filter is used for classification.

Since MSS algorithm employed in our study has taken care of both spatial and spectral features, it has conveniently outclassed texture based analysis for flood assessment. MSS takes both surface roughness and dielectric constant into account and hence proves to be better classification method compared to GLCM. It is inferred from the graph shown in figure 11.

5. Conclusions and discussions

Synthetic aperture radar images exploited in our image segmentation methods have allowed us to obtain the information of flood prone regions effectively. Prior to this, speckle removal filters are applied on SAR image to ensure that the image is free from speckle noise. Since, SAR reflectance is dependent on smoothness of the surface, sometimes flowing water in the river may not appear dark as the still water rather appear like a part of land region (Eisuke 2012). The dielectric properties of the surface also contribute to the SAR reflectance (Freeman and Durden 1998). Hence these characteristic features are handled by GLCM texture properties and spatial-range mean shift segmentation. In comparison with GLCM, accuracy assessment result is quite promising with mean shift segmentation for flood mapping. This study has shown that flooded and non-flooded region obtained from SAR image and analysing it with before flood (LISS-III) image helps to get the land cover regions that are affected by flood. Hence this is very valuable for the decision makers who plan for flood management measures.

References

Canada Centre for Remote Sensing (CCRS), Advance Radar Polarimetric Tutorial 2011 http://gs.mdacorporation.com/SatelliteData/Radarsat2/Radarsat2.aspx.

Chakraborty D, Sen G and Kand H S 2009 High-resolution satellite image segmentation using Holder exponents; *J. Earth Syst. Sci.* **118(5)** 609–617.

Chenghu Z, Jiancheng L, CunJian Y, Baolin Li and Shixin W 2000 Flood monitoring using multi-temporal AVHRR and RADARSAT imagery; *Photogramm. Engg. Rem. Sens.* **66(5)** 633–638.

Chunming H, Huadong G, Shao Y and Liao J 2005 Detection of the flood boundary in SAR image using texture; *Proc. Geosci. Rem. Sens. Symp.* Seoul, Korea, **5** 3697–3699.

Comaniciu D and Meer P 2002 Mean Shift: A robust approach towards feature space analysis; *IEEE Trans. Pattern Analysis and Machine Intelligence* **24(5)** 603–619.

Durand M J, Gimonet B J and Perbos J R 1987 SAR data filtering for classification; *IEEE Trans. Geosci. Rem. Sen.* **25** 629–637.

Duc V B 2006 Advantage of the remote sensing data utilization in studying inundation risks in terms of Land-use; *IEEE Int. Conf. Geosci. Rem. Sens. Symp.*, pp. 279–282.

Eisuke K 2012 Basic principle of Synthetic-Aperture Radar (SAR); *8th Sentinel Asia System (SAS) Operation Training*, Bangkok.

Freeman A and Durden S 1998 A three component scattering model for polarimetric SAR data; *IEEE Trans. Geosci. Rem. Sens.* **36** 963–973.

Frost J A, Shanmugan K S and Holtzman J C 1982 A model for radar images and its application to adaptive digital filtering of multiplicative noise; *IEEE Trans. Pattern Anal. Machine Intell. PAMI* **4** 157–165.

Gamba P and Aldrighi M 2012 SAR data classification of urban areas by means of segmentation techniques and ancillary optical data; *IEEE J. Sel. Top. Appl. Earth Obs. Rem. Sens.* **5(4)** 1140–1148.

Herrera-Cruz V and Koudogbo F 2009 TerraSAR-X Rapid mapping for flood events; *Proc. Int. Soc. Photogramm. Rem. Sens. (Earth Imaging for Geospatial Information)*, Hannover, Germany, pp. 170–175.

Huang S Q 2008 Change mechanism analysis and integration change detection method on SAR images, *The International Archives of the Photogrammetry, Remote Sensing and Spatial Information Sciences. Vol. XXXVII. Part B7*, Beijing.

Jarabo A P, Rosa Z M, De la Mata-Moya D, Vicen B and Maldonado B S 2011 Spatial-range mean-shift filtering and segmentation applied to SAR images; *IEEE Trans. Instrumentation and Measurement* **60(2)** 584–597.

Konstantinos G D 2005 Mean Shift Clustering.

Kussul N, Andrii S and Serhiy S 2008 Intelligent computations for flood monitoring; *14th Int. Conf. of Knowledge-Dialogue-Solution*, Varna, Bulgaria, pp. 48–54.

Lee J S 1981 Speckle analysis and smoothing of Synthetic Aperture Radar images; *Comp. Graphics and Image Processing* **17(1)** 24–32.

Lopes A, Nezry E, Touzi R and Laur H 1990 Maximum a-posteriori speckle filtering and first order texture models in SAR Images; *10th Ann. Int. Symp. Geosci. Rem. Sens.*, pp. 2409–2412.

Mansourpour M, Rajabi M A and Blais J A R 2006 Effects and performance of speckle noise reduction filters on active radar and SAR images; *Proc. ISPRS Symp. on Topographic Mapping from Space (with Special Emphasis on Small Satellites)* Ankara, Turkey **XXXVI-1/W41**.

Matgen P, Hostache R, Schumann G, Pfister L, Hoffmann L and Savenije H H G 2011 Towards an automated SAR-based flood monitoring system: Lessons learned from two case studies; *Phys. Chem. Earth* **36(7/8)** 241–252.

Patel P, Srivastava H S and Navalgund R R 2009 Use of synthetic aperture radar polarimetry to characterize wetland targets of Keoladeo National Park, Bharatpur, India; *Curr. Sci.* **97(4)** 529–537.

Shamaomaa H, Kerleb N and Alkemab D 2006 Extraction of flood-modelling related base-data from multisource remote sensing imagery; *Proc. ISPRS Comm VII Symp.*, Enschede, Netherlands **36(7)**.

Sheng Y and Xia Z 1996 A comprehensive evaluation of filters for radar speckle suppression; *Proc. IGARSS* **2** 1559–1561.

Srivastava H S, Patel P, Sharma K P and Krishnamurthy Y V N 2009 Explored and demonstrated potential applications of multiparametric Synthetic Aperture Radar in wetland studies in context of Keoladeo National Park, Bharatpur, India; In: *Proceedings Second Annual Research Seminar – KNP*, Bharatpur, India, pp. 1–30.

Srivastava H S, Patel P and Navalgund R R 2006 Application potentials of synthetic aperture radar interferometry for land-cover mapping and crop-height estimation; *Curr. Sci.* **91(6)** 783–786.

Stehman S V 1995 Thematic map accuracy assessment from the perspective of finite population sampling; *Int. J. Remote Sens.* **16** 589–593.

MS received 9 July 2012; revised 11 October 2012; accepted 10 January 2013